Published in final edited form as:
Magn Reson Med. 2014 January ; 71(1): . doi:10.1002/mrm.24641.

A Method for High Resolution Imaging of Creatine In vivo using Chemical Exchange Saturation Transfer (CrCEST)

Feliks Kogan[1,2], **Mohammad Haris**[1], **Anup Singh**[1], **Kejia Cai**[1], **Catherine Debrosse**[1], **Ravi Prakash Reddy Nanga**[1], **Hari Hariharan**[1], and **Ravinder Reddy**[1]

[1]Center for Magnetic Resonance and Optical Imaging, Department of Radiology, University of Pennsylvania, B1 Stellar-Chance Labs, 422 Curie Boulevard, Philadelphia, PA 19104

[2]Department of Bioengineering, University of Pennsylvania, Philadelphia, PA, USA

Abstract

Purpose—To develop a chemical exchange saturation transfer (CEST) based technique to measure free creatine (Cr) and to validate the technique by measuring the distribution of Cr in muscle with high spatial resolution before and after exercise.

Methods—Phantom studies were performed to determine contributions from other creatine kinase metabolites to the CEST effect from Cr (CrCEST). CEST, T_2, magnetization transfer ratio (MTR) and ^{31}P magnetic resonance spectroscopy (MRS) acquisitions of the lower leg were performed before and after plantar flexion exercise on a 7T whole-body MR scanner on healthy volunteers.

Results—Phantom studies demonstrated that while Cr exhibited significant CEST effect there were no appreciable contributions from other metabolites. In healthy human subjects, following mild plantar flexion exercise, increases in CrCEST were observed, which recovered exponentially back to baseline. This technique exhibited good spatial resolution and was able to differentiate differences in muscle utilization among subjects. CrCEST results were compared with ^{31}P MRS results showing good agreement in the Cr and PCr recovery kinetics.

Conclusion—Demonstrated a CEST based technique to measure free creatine changes in *in vivo* muscle. CrCEST imaging can spatially map changes in creatine concentration in muscle following mild exercise. This may serve as a tool for the diagnosis and treatment of various disorders affecting muscle.

Keywords

CEST; Creatine; Muscle; Chemical Exchange; Endogenous Contrast

INTRODUCTION

The creatine kinase (CK) reaction plays a vital role in the muscle energetics(1).

$$\mathrm{Cr}+\mathrm{ATP} \leftrightarrow \mathrm{ADP}+\mathrm{PCr}+H^{+} \quad [1]$$

Adenosine triphosphate (ATP), derived from the conversion of phosphocreatine (PCr) to creatine (Cr) by the CK reaction, provides an essential chemical energy source that governs

Address for Correspondence: Feliks Kogan, Center for Magnetic Resonance and Optical Imaging (CMROI), Department of Radiology, University of Pennsylvania, B1 Stellar-Chance Laboratories, 422 Curie Boulevard, Philadelphia, PA 19104-6100, Tel: (215) 898-2045, Fax: (215) 573-2113, fkogan@seas.upenn.edu.

muscle contraction (2,3). While ATP represents the fundamental energy currency, PCr serves as the reservoir of cellular energy. During exercise, PCr is depleted to maintain the ATP supply leading to an increase Cr concentration.

Magnetic Resonance (MR) techniques have been used extensively for noninvasive functional investigations of exercising muscle metabolism and are becoming increasingly more important for studying muscular diseases(4). ^{31}P Magnetic Resonance Spectroscopy (MRS) was the first and is currently the most utilized method to study oxidative metabolism of skeletal muscle(5–8). Additionally, intracellular pH can also be measured noninvasively from the chemical shift of the P_i peak(9).

The ability of ^{31}P MRS to measure high-energy phosphate compounds as well as pH changes has made it a great tool for studying metabolic abnormalities associated with various myopathies(10–12) as well as cardiac energetics(13,14). ^{31}P MRS has also provided key information about secondary problems of muscle metabolism associated with common conditions such as heart failure(15,16), peripheral vascular disease(17), and thyroid disease(18).

^{1}H MRS can only measure total creatine and cannot differentiate between PCr and Cr and thus has little application towards measuring energy metabolism (19,20). While there have been a limited amount of ^{1}H MRI studies utilizing T_2 relaxation rates to study muscle energetics, the mechanism of the T_2 increases in muscle exercise is still poorly understood(21–23).

Although these MR methods have been critical to our understanding of muscle energetics, they also suffer from several drawbacks. ^{31}P MRS, like all spectroscopy techniques, suffers from poor spatial resolution as well as low sensitivity. Furthermore, neither ^{1}H MRS nor ^{31}P MRS can measure free Cr.

Chemical exchange saturation transfer (CEST) is new sensitivity enhancement mechanism to indirectly detect metabolite content based on exchange-related properties (24,25). In a CEST experiment, saturated magnetization from exchangeable protons on a pool of solute molecules is transferred to a much larger pool of bulk water protons. This reduction in water signal results in a solute concentration dependent contrast in CEST water images(26–28). CEST has been used to image endogenous mobile proteins and peptidesin biological tissue by selectively saturating their labile protons (29–31).

More recently, it has been shown that Cr exhibits a concentration dependent CEST effect between its amine ($-NH_2$) and bulk water protons (32–34). Cr amine protons have an exchange site at ~1.8 ppm from water and the CEST effect from creatine is linearly proportional to the Cr concentration in the physiological pH range(34).

In this work, for the first time, we demonstrated the potential of measuring the CEST effect from Cr (CrCEST) in spatial and temporal mapping of muscle energetics. Phantom studies were performed to demonstrate minimal contributions from other creatine kinase reaction metabolites to the observed CrCEST under the same saturation parameters used in the skeletal muscle experiments *in vivo*. We also demonstrated that CrCEST has over three orders of magnitude higher sensitivity compared to ^{31}P MRS. Changes in CrCEST in calf muscles of healthy human volunteers were mapped following plantar flexion exercises. Additionally, we measured changes in magnetization transfer ratio (MTR) and T_2 following exercise. Finally, we showed complementary recovery kinetics of CrCEST and ^{31}P MRS under the same exercise conditions.

MATERIALS AND METHODS

MRI Scans

All imaging experiments were performed on a 7T whole body scanner (Siemens Medical Systems, Erlangen, Germany). A 32 Channel ^{1}H head coil was used for phantom imaging while a 28 channel ^{1}H knee coil was utilized for Calf imaging. Localized B_0 shimming was performed with second order shims using the Siemens product interactive shim program to keep reported water line widths to less than 45Hz (0.15 ppm). ^{31}P MRS was performed with a custom built 7 cm diameter ^{31}P transmit/receive surface coil. An MR compatible pneumatically controlled foot pedal was designed and used for plantar flexion exercise (figure 1a). The pressure applied to the pedal was controlled with a pneumatic gauge and held constant across all subjects. In CEST imaging experiments, we utilized a 500 ms long saturation pulse train consisting of a series of 99.6 ms Hanning windowed saturation pulses (with peak amplitude set to provide desired $B1_{rms}$) with a 400 μs interpulse delay (99.6% duty cycle, 100 ms pulse train), followed by a single shot RF spoiled gradient echo (GRE) readout with centric phase encoding order. The excitation bandwidth of this saturation pulse train was 10 Hz for a 500 ms saturation duration with a 1% bandwidth of 40 Hz. A chemical shift selective fat saturation pulse was applied prior to image readout to reduce the signal from fat in the muscle. CEST images of the lower leg at varying saturation amplitude and duration were acquired on a healthy volunteer in order to empirically optimize muscle CEST saturation parameters within the constraints of imaging of humans at 7T. Water saturation shift reference (WASSR) images and B_1 maps were collected, as described previously (35,36), for all CEST studies before and after exercise to correct for B_0 and B_1 inhomogeneities. WASSR images were collected from −0.5 ppm to 0.5 ppm with a step size of 0.05 ppm and saturation pulse train amplitude, B_{1rms} of 12.4 Hz (0.3 μT) and 200 ms duration using the same sequence as used for CEST imaging and identical readout parameters. Cr amine protons have a chemical shift of 1.8 ppm downfield from water and thus CEST images were collected in a frequency shift range with respect to the water resonance of +1.5 ppm to +2.1 ppm and −1.5ppm to −2.1 ppm with a 0.3 ppm step size to calculate $CrCEST_{asym}$ and allow for adequate B_0 inhomogeneity correction.

Phantom Imaging

All phantoms were prepared in PBS and imaged at 37°C. Samples of 10 mM Cr, 15 mM PCr, 10 mM ATP, and 10 mM ADP were prepared to observe any potential contributions the Cr CEST effect. The imaging parameters were as follows: slice thickness = 4 mm, flip angle = 10°, TR = 7.1 ms, TE = 3.5 ms, field of view = 100 × 100 mm^2, matrix size = 192 × 192, with one saturation pulse every 8 seconds. CEST images were collected with a B_{1rms} of 123 Hz (2.9 μT) and 500 ms duration.

Human Studies

All Studies were conducted under an approved Institutional Review Board protocol of the University of Pennsylvania. Written informed consent from each volunteer was obtained after explaining the study protocol. CEST, T_2/MTR and ^{31}P MRS acquisitions of the calf were performed in separate exercise bouts at 7T on healthy volunteers (n=8, 5 male, 3 female, ages 19–30) with various activity levels (sedentary to active). Additionally, ^{1}H MRS was performed on one healthy subject.

For each methodology, baseline imaging was performed for 2 minutes, followed by 2 minutes of mild plantar flexion exercise and then 8 minutes of post exercise imaging. Calf CEST imaging was performed with the same CEST saturation pulse train described for the phantoms and the following imaging parameters: slice thickness = 4 mm, flip angle = 10°, TR = 6.1 ms, TE = 2.9 ms, field of view = 130 × 130 mm^2, matrix size = 128 × 128. To

compute MTR maps, the same sequence with a saturation duration of 1 second (B_{1rms}= 2.9 μT) was performed at 20 ppm along with a sequence without selective saturation. To obtain T_2 maps, a T_2 spin-echo prepared FLASH sequence was used with the parameters mentioned above at echo times of 2.4, 12.5, 25, 37.5, and 50 ms. Additionally, a z-spectra acquisition was performed on the lower leg of one healthy subject at baseline from −4.0 ppm to 4.0 ppm with a step size of 0.2 ppm, a B_{1rms} of 123 Hz (2.9 μT) and a 500 ms duration. ^{1}H MRS spectra were obtained from a region in the lateral gastrocnemius muscle using a standard point resolved spectroscopy (PRESS)(37) localization technique with the following parameters: voxel size = 10 × 20 ×10 mm^3, spectral width = 3 kHz, number of points = 2048, average = 16, TE = 20 ms, and TR = 3 s. Finally, non-localized ^{31}P MRS was performed with a 7-cm diameter surface coil positioned on the calf and the following parameters: spectral width = 5 kHz, number of points = 512, averages = 4, and TR = 3 s. In order to determine the depth of penetration of the ^{31}P surface coil, a 2 M sodium phosphate phantom was imaged using a ^{31}P ultra-short echo time (UTE) sequence with the following parameters: FOV =140 × 140 mm^2, matrix size = 64 × 64, flip angle = 20°, TR = 50 ms, TE = 100 μs, averages = 4.

Data Processing

All image processing and data analysis was performed using in-house written MATLAB (version 7.5, R 2007b) scripts. B_0 maps were used to generate corrected CEST images (±1.8 p.p.m.) using the WASSR method(35). Similarly, B_1 maps were created from two images obtained using preparation square pulses with flip angles of 30° and 60°. A B_1 calibration curve for muscle was developed from calf CEST data at varying saturation amplitudes and used in conjunction with B_1 maps to correct for B_1 inhomogeneities(36). CEST contrast was computed by subtracting the normalized magnetization signal at the Cr proton frequency (Δω = +1.8 ppm), from the magnetization at the corresponding reference frequency symmetrically at the opposite side of the water resonance (−Δω)(38)

$$CEST_{asym}=\frac{M_{sat}(-\Delta\omega)-M_{sat}(+\Delta\omega)}{M_{sat}(-\Delta\omega)} \quad [2]$$

Anatomical images were manually segmented and applied to $CrCEST_{asym}$ maps in order to determine the $CrCEST_{asym}$ changes in each individual muscle group before and after exercise. Similarly, MTR maps were computed by

$$\mathrm{MTR}=\frac{M_0-M_{\mathrm{Sat}}}{M_0}\times 100\% \quad [3]$$

Where M_0 is the magnetization without saturation and M_{Sat} is the magnetization with a saturation pulse applied at Δω = 20 ppm. T_2 maps were created by fitting images acquired with various echo times to $S=Soe^{-TE/T2}$ and solving for T_2 on a pixel-wise basis. Eddy current corrected ^{1}H MRS and ^{31}P MRS Spectra were phased and baseline corrected and then fitted using nonlinear squares methods with Lorentzian or Gaussian functions.

RESULTS

In vivo CEST parameter optimization

Our experimental setup is shown in figure 1a. The anatomical image of an axial slice of the lower leg with various muscle groups segmented is shown in figure 1b. The $CEST_{asym}$ map overlaid on the anatomical image showed fairly uniform $CrCEST_{asym}$ at baseline (Fig. 1c–1e). The z-spectra and CEST asymmetry plot from the soleus muscle at baseline was broad

and showed maximum CEST contrast at ~ 1.8 ppm (Fig. 1f,g). Figure 1i shows a plot of the $CEST_{asym}$ as well as the signal-to-noise ratio (SNR) of the anatomical image following saturation as a function of saturation pulse B_{1rms} for a 500 ms pulse train. Increasing B_{1rms} leads to an increase in labile proton saturation efficiency that increases the $CEST_{asym}$. However, when the saturation efficiency is already high, increases in B_{1rms} result in increased direct water saturation, which decreases the $CEST_{asym}$. Increases in B_{1rms} also decrease the SNR of images. Thus, in order to maximize $CEST_{asym}$ and SNR, a saturation pulse train with B_{1rms} of 123 Hz (2.9 μT) and 500 ms duration was chosen for this study. We define the CEST effect at $\Delta\omega = 1.8$ ppm using those saturation parameters as CrCEST.

Potential contributions from other creatine kinase metabolites

All the major metabolites of the creatine kinase reaction have amine group protons which exchange with water protons. With these *in vivo* empirically optimized experimental parameters, a 4.1% (±0.2%) $CrCEST_{asym}$ was observed from 10mM Cr, while negligible CrCEST effects were observed from 15 mM PCr (0.3±0.1%), 10 mM ATP(0.2±0.1%), and 10 mM ADP(0.3±0.1%) (fig 1h). This is predominantly due to their unfavorable exchange rates and differences in the chemical shifts of their amine protons. At physiological pH and temperature, ATP and ADP, have much slower exchange rates (120±50 s^{-1}) than Cr (950±100 s^{-1})(34). Similarly, PCr has a much slower exchange rate (140±50 s^{-1} at its 2.5 ppm peak and 120±50 s^{-1} for its 1.8 ppm peak) and thus has minor effects at 1.8 ppm with the parameters used(34).

In vivo human studies

Plantar flexion exercise led to an increase in the $CrCEST_{asym}$ in all subjects. Figure 2a shows $CrCEST_{asym}$ maps for the same subject before and after mild plantar flexion exercise with a temporal resolution of 48 seconds. The time dependence of the mean $CrCEST_{asym}$ for each segmented muscle group (fig 1b) is plotted in figure 2b along with error bars representing the standard deviation in $CrCEST_{asym}$ in each region. The principle muscles involved in plantar flexion are located in the posterior compartment of the leg and include the soleus muscle as well as the medial (MG) and lateral (LG) heads of the gastrocnemius muscles. Thus, plantar flexion exercise is expected to increase creatine levels primarily in the soleus and gastrocnemius muscles of the leg. This is exhibited in $CrCEST_{asym}$ maps, which show that the majority of $CrCEST_{asym}$ increases were localized in the posterior compartment of the leg. Whereas the CEST maps showed fairly uniform $CrCEST_{asym}$ at baseline, the first post-exercise map showed a 6.7%(±1.0%) and 7.2%(±0.8%) increase in $CrCEST_{asym}$ in the medial and lateral gastrocnemius muscles, respectively, following exercise. A 2.6%(±0.9%) increase was observed in the soleus, the other major muscle of the posterior compartment. The tibialis anterior (AT) is predominantly involved in dorsiflexion and as a result, less than a 1% increase in $CrCEST_{asym}$ was observed. The $CrCEST_{asym}$ in all the muscles was seen to recover exponentially back to baseline after roughly three time points or about 2 minutes. Both T_2 and MTR maps did not show any significant differences ($\Delta T_2 < 0.5$ ms, $\Delta MTR < 1.0\%$) [data not shown].

Figure 3 shows CrCEST results from a different subject. Unlike the first subject, these CEST maps show that the majority of $CrCEST_{asym}$ increase is localized in the soleus muscle and the muscle is well segmented in the first post-exercise CEST Map. A 5.2% (±1.1%) increase in $CrCEST_{asym}$ was observed in the soleus muscle compared to 1.4% (±0.5%) and 1.6% (±0.5%) detected in the medial and lateral gastrocnemius muscles respectively. Similar to subject 1, the $CrCEST_{asym}$ in all the muscles recovered exponentially back to baseline in about 2 minutes (fig 3b). In all volunteers, no significant changes were observed in the T_2 ($\Delta T_2 < 0.5$ ms) and MT ($\Delta MTR < 1.0\%$) maps following exercise [data not shown]. This

demonstrates that this method can detect subject dependent changes in muscle group recruitment during exercise.

A free induction decay (fid) was used for ^{31}P MRS acquisition in the current study, and thus the signal was unlocalized. The ^{31}P MRS surface coil excitation profile measured using phantoms is shown in figure 4a overlaid on an anatomical image of the lower leg. The majority of the ^{31}P MRS signal comes from the gastrocnemius muscle with minor contributions from the soleus muscles. ^{31}P MRS spectra were acquired 2 minutes before and 8 minutes after exercise with a temporal resolution was 12 seconds per fid spectrum. A stacked plot of every alternate spectra acquired is shown for subject 1 in figure 4b. A decrease in the PCr peak area following exercise is evident, which recovers back to the pre-exercise levels in about 2 minutes. The size and area of the three ATP peaks stayed constant before and after this exercise. The P_i peak increased after exercise and then quickly decayed back to baseline. No shift or splitting of the P_i peak was observed indicating that there were negligible pH changes. Finally, when the PCr area was integrated to have an equal temporal resolution to that of CEST measurements, a very good agreement was observed in the rates at which the $CrCEST_{asym}$ from the region of interest pictured in fig 4a and the ^{31}P MRS signal recovered to baseline (fig 4c).

Time dependent ^{1}H MRS provides insight into changes in total creatine(tCr), which is the combined signal from Cr and PCr. Figure 5a shows the spectroscopy voxel location overlaid on the anatomical image. Figure 5b shows the ^{1}H MR Spectrum as a function of time before and after exercise with a temporal resolution of 48 seconds equal to that of the CEST measurements. As seen in figure 5c, the plot of the integrated tCr peak as a function of time shows no changes before or after exercise. This is due to the fact that the concentrations of Cr and PCr are tightly coupled in the creatine kinase reaction. Thus, a decrease in PCr will lead to an equivalent increase in Cr and thus the total Cr peak observed in ^{1}H MRS will remain constant.

Figure 6 shows a summary of data from all 8 volunteers. The ^{31}P MRS PCr peak integral as a function of time is shown in figure 6a. The mean $CrCEST_{asym}$ in the region of interest corresponding to the ^{31}P MRS surface coil excitation profile [see figure 4a] is plotted as a function of time for each subject in figure 6b. There was some subject variability in regards to the level and involvement of each muscle group. However, the two figures show good agreement in the rate and shape at which they recover back to baseline following exercise for each subject. To compare the $CEST_{asym}$ and ^{31}P MRS results, the % decrease in ^{31}P MRS signal from baseline at the first integrated measurement following exercise was used to determine the decrease in PCr based on a 33 mM PCr baseline concentration(8). As the total Cr remains constant, the decrease in PCr concentration should equate to an equivalent increase in Cr concentration. Thus we can compare the average change in the $CEST_{asym}$ in the region of interest to the calculated change in Cr concentration across all subjects (fig 6c). This produces a slope of 0.84 % $CrCEST_{asym}$/mM Cr with an R^2 value 0.75.

DISCUSSION

The results of this work provide the first evidence that the CEST effect from Cr can be used to noninvasively measure creatine with high spatial resolution in muscle following exercise.

The $CrCEST_{asym}$ observed from Cr in phantom experiments was lower than what we observed in *in vivo* experiments. This is due to our definition of $CEST_{asym}$ which uses the $M_{sat}(-\Delta\omega)$ for normalization as it has a higher dynamic range. As the T_2 of Cr phantoms is long (~800 ms), there is very little direct water saturation and as a result $M_{sat}(-\Delta\omega)$ is very close to M_0, the magnetization without selective saturation. When M_0 is used to normalize

in vivo images, the $CEST_{asym}$ in muscle decreases by a factor of ~2. This would yield a $CEST_{asym}$ of 0.42% $CEST_{asym}$/mM Cr, which would be in good agreement with phantom results.

Enhanced sensitivity is one of the inherent characteristics of the CEST methods. Based on the 0.42% CEST/mM Cr and muscle water proton concentration (82.5M), 1 mM Cr signal leads to 346 mM change in water. Considering that the receptivity of ^{31}P NMR compared to that of ^{1}H NMR is 0.066, we expect an increase in sensitivity of ~ 5240 with CEST. Thus compared to ^{31}P NMR, CrCEST has about 3 orders of magnitude higher sensitivity.

Prolonged strenuous exercise can lead to glycogen breakdown to provide substrates for glycolysis which through the combined production of lactate and ATP hydrolysis lowers pH (39,40). This decrease in pH will decrease the exchange rate between Cr amine protons and water protons which will lead to a lower CEST contrast. As the performed exercise was mild and aerobic, most of the energy was obtained from the oxidative TCA cycle and lactate levels and pH remained the same(41). This was validated with ^{31}P MRS, which showed no shifts in the P_i peak. Finally, a decrease in pH, had it occurred, would lead to a decrease in $CrCEST_{asym}$, and thus would underestimate the increase in Cr post exercise. Furthermore, in previous work, glycogen has been shown in vitro and in liver *in vivo* to exhibit a CEST effect around 1.0 ppm from exchange of its hydroxyl (-OH) protons with bulk water(42). However, as no pH changes were observed in ^{31}P MRS, we assume that there is no glycogen contribution to the observed CrCEST changes in the mild exercise employed in this study. Hence, glycogen is not expected to contribute to the observed changes in $CrCEST_{asym}$ following plantar flexion exercise employed in this study.

Changes in pH provide both an opportunity and a confounding effect for CrCEST. It is well known that the Cr concentration returns to baseline faster than the pH(43,44). During strenuous exercise when the pH becomes acidic (<7), the $CrCEST_{asym}$ will decrease below baseline when the Cr concentration has recovered and then slowly increase back to the baseline $CrCEST_{asym}$ as the pH normalizes. This decrease below the baseline $CrCEST_{asym}$ may provide information about pH changes in the muscle. Further studies will be needed to characterize the effects of pH on the CrCEST effect of exercised muscle.

Magnetization transfer, which is caused by the bound pool of water from rigid macromolecules, also may have an effect on the CEST contrast. However, as we did not observe any changes on the calculated MTR maps before and after exercise, we do not expect any MTR contamination of the measured increase in $CrCEST_{asym}$ following exercise in this study.

Phantom experiments showed that ATP, ADP, and PCr do not contribute to the CrCEST effect at 1.8 ppm under the saturation parameters used in this study. ^{31}P MRS also showed no change in ATP following exercise. Since ADP concentration is too small (< 1mM) to be reliably measured, its contribution to CrCEST is negligible. Finally, there is a decrease in PCr concentration following exercise which would have decreased the observed $CrCEST_{asym}$ had PCr exhibited an observable CEST effect at 1.8 ppm under these parameters. Also, any changes in pH, had they occurred would reduce the already slow exchange rates of PCr, ATP and ADP amine protons, and further reduce their contribution to the CrCEST effect. Amide protons, which are present in the calf muscle and have been used with CEST imaging, have a chemical shift of 3.5 ppm and slow exchange rate (< 50 s^{-1}) (30,45). However, a z-spectra from muscle acquired with the saturation parameters used in this study showed less than a 1 % $CEST_{asym}$ at $\Delta\omega = 3.5$ ppm (Fig. 1g). As a minimal CEST effect is seen at 3.5 ppm with these parameters, amide protons contributions to the CrCEST effect at 1.8 ppm are expected to be small. Since there was no change in pH, T_2, or MTR

and the CEST effects from other creatine kinase reaction metabolites were negligible, it can be concluded that the observed changes in $CrCEST_{asym}$ following plantar flexion exercise presented in this study are predominantly due to changes in muscle Cr concentration.

It is also necessary to point out several potential limitations of the study. Since, a dual tuned $^{31}P/^{1}H$ 7T coil was not available, it was not possible to obtain a localized ^{31}P spectrum of the exact slice acquired with CEST imaging or localize it to a specific muscle. Thus, the majority of the phosphorus ^{31}P MRS signal originated from the gastrocnemius muscles from a large area of the calf. As a result, comparisons made between $CrCEST_{asym}$ and ^{31}P MRS are estimates as the spectral data is obtained from a larger volume of the leg. Nonetheless, there was good agreement in the rates and shape at which the $CrCEST_{asym}$ and ^{31}P MRS signal recovered to baseline across all subjects. Subjects with smaller increases in $CrCEST_{asym}$ post exercise similarly had smaller decreases in their PCr peak. Furthermore, in subjects where $CrCEST_{asym}$ changes were localized mainly in the soleus muscles with smaller changes observed in the gastrocnemius muscles, smaller decreases were observed in the ^{31}P MRS measured PCr peak levels post exercise.

Also, CEST, T_2, MTR and ^{31}P MRS data were not collected concurrently and as a result there may have been differences in muscle changes between exercise bouts. However, since subjects were healthy volunteers and exercise was mild, these variations are expected to be small. Finally, the temporal resolution used for CrCEST mapping in this work is too long to adequately characterize creatine kinase kinetics for clinical application. However, the feasibility of measuring Cr concentration changes is demonstrated. There is potential for improving the temporal resolution by decreasing the shot TR and resolution. Work by many groups is also being conducted on methods to reduce CEST scan times while maintaining adequate B_0 correction. These advances will allow this technique to be clinically applicable.

In summary, it is feasible to use CEST imaging to measure changes in Cr concentration in muscle following plantar flexion exercise. The observed increases in $CrCEST_{asym}$ following exercise were due mainly to increases in Cr concentration in this study. CrCEST exhibited a sensitivity enhancement of over 3 orders of magnitude compared to ^{31}P MRS. Further, $CrCEST_{asym}$ maps showed good spatial resolution and were able to differentiate varying muscle usage in different subjects. There was good agreement between the recovery kinetics of ^{31}P MRS and $CrCEST_{asym}$ following exercise. While the experiments demonstrated in this work were performed at 7T, the favorable exchange rate of Cr amine protons would allow for these studies to be performed at 3T as well. This may require further work to optimize saturation parameters.

Future studies using this approach may provide new insights into muscle energetics and can serve as a tool for the diagnosis and treatment of muscle disorders. In addition, this technique has the potential to provide key information about primary disorders of muscle metabolism as well as the secondary complications of muscle metabolism associated with common conditions such as heart failure, renal failure, and peripheral vascular disease. In addition to studies of skeletal muscle, CrCEST may also have applications in studies of cardiac energetics as well as functional studies of the brain.

Acknowledgments

We gratefully acknowledge V. Kassey and A. Bonner for their help in designing and building the MR compatible exercise setup. We thank D. Reddy for his help with human studies. This work was supported by a NIBIB supported resources center grants P41EB015893, P41EB015893S1 and a training grant T32EB009384.

References

1. Chance B, Williams GR. Respiratory enzymes in oxidative phosphorylation.3. The steady state. J Biol Chem. 1955; 217(1):409–427. [PubMed: 13271404]
2. Cain DF, Davies RE. Breakdown of adenosine triphosphate during a single contraction of working muscle. Biochem Biophys Res Commun. 1962; 8(5):361–366. [PubMed: 13875588]
3. Davies RE. A molecular theory of muscle contraction - calcium-dependent contractions with hydrogen bond formation plus atp-dependent extensions of part of myosin-actin cross-bridges. Nature. 1963; 199(489):1068–1074. [PubMed: 14066941]
4. Bendahan D, Giannesini B, Cozzone PJ. Functional investigations of exercising muscle: a noninvasive magnetic resonance spectroscopy-magnetic resonance imaging approach. Cell Mol Life Sci. 2004; 61(9):1001–1015. [PubMed: 15112049]
5. Hoult DI, Busby SJW, Gadian DG, Radda GK, Richards RE, Seeley PJ. Observation of tissue metabolites using P-31 nuclear magnetic-resonance. Nature. 1974; 252(5481):285–287. [PubMed: 4431445]
6. Dawson MJ, Gadian DG, Wilkie DR. Muscular fatigue investigated by phosphorus nuclear magnetic-resonance. Nature. 1978; 274(5674):861–866. [PubMed: 308189]
7. Ingwall JS. Phosphorus nuclear magnetic-resonance spectroscopy of cardiac and skeletal-muscles. Am J Phys. 1982; 242(5):H729–H744.
8. Kemp GJ, Meyerspeer M, Moser E. Absolute quantification of phosphorus metabolite concentrations in human muscle in vivo by P-31 MRS: a quantitative review. NMR Biomed. 2007; 20(6):555–565. [PubMed: 17628042]
9. Burt CT, Glonek T, Barany M. Analysis of phosphate metabolites, intracellular ph, and state of adenosine-triphosphate in intact muscle by phosphorus nuclear magnetic-resonance. J Biol Chem. 1976; 251(9):2584–2591. [PubMed: 4452]
10. Argov Z, Bank WJ. Phosphorus magnetic-resonance spectroscopy (P-31 MRS) in neuromuscular disorders. Ann Neurol. 1991; 30(1):90–97. [PubMed: 1834009]
11. Argov Z, Lofberg M, Arnold DL. Insights into muscle diseases gained by phosphorus magnetic resonance spectroscopy. Muscle Nerve. 2000; 23(9):1316–1334. [PubMed: 10951434]
12. Tarnopolsky MA, Parise G. Direct measurement of high-energy phosphate compounds in patients with neuromuscular disease. Muscle Nerve. 1999; 22(9):1228–1233. [PubMed: 10454718]
13. Neubauer S, Krahe T, Schindler R, Horn M, Hillenbrand H, Entzeroth C, Mader H, Kromer EP, Riegger GAJ, Lackner K, Ertl G. P-31 magnetic-resonance spectroscopy in dilated cardiomyopathy and coronary-artery disease - altered cardiac high-energy phosphate-metabolism in heart-failure. Circulation. 1992; 86(6):1810–1818. [PubMed: 1451253]
14. Yabe T, Mitsunami K, Inubushi T, Kinoshita M. Quantitative measurements of cardiac phosphorus metabolites in coronary-artery disease by P-31 magnetic-resonance spectroscopy. Circulation. 1995; 92(1):15–23. [PubMed: 7788910]
15. Massie BM, Conway M, Rajagopalan B, Yonge R, Frostick S, Ledingham J, Sleight P, Radda G. Skeletal-muscle metabolism during exercise under ischemic conditions in congestive heart-failure - evidence for abnormalities unrelated to blood-flow. Circulation. 1988; 78(2):320–326. [PubMed: 3396168]
16. Mancini DM, Coyle E, Coggan A, Beltz J, Ferraro N, Montain S, Wilson JR. Contribution of intrinsic skeletal-muscle changes to P-31 NMR skeletal-muscle metabolic abnormalities in patients with chronic heart-failure. Circulation. 1989; 80(5):1338–1346. [PubMed: 2805270]
17. Kemp GJ, Hands LJ, Ramaswami G, Taylor DJ, Nicolaides A, Amato A, Radda GK. Calf muscle mitochondrial and glycogenolytic atp synthesis in patients with claudication due to peripheral vascular-disease analyzed using P-31 magnetic-resonance spectroscopy. Clin Sci. 1995; 89(6): 581–590. [PubMed: 8549076]
18. Argov Z, Renshaw PF, Boden B, Winokur A, Bank WJ. Effects of thyroid-hormones on skeletal-muscle bioenergetics – in vivo P-31 magnetic-resonance spectroscopy study of humans and rats. J Clin Invest. 1988; 81(6):1695–1701. [PubMed: 3384946]
19. Bottomley PA, Lee YH, Weiss RG. Total creatine in muscle: Imaging and quantification with proton MR spectroscopy. Radiology. 1997; 204(2):403–410. [PubMed: 9240527]

20. Rico-Sanz J, Thomas EL, Jenkinson G, Mierisova S, Iles R, Bell JD. Diversity in levels of intracellular total creatine and triglycerides in human skeletal muscles observed by H-1-MRS. J Appl Physiol. 1999; 87(6):2068–2072. [PubMed: 10601151]
21. Fisher MJ, Meyer RA, Adams GR, Foley JM, Potchen EJ. Direct relationship between proton t2 and exercise intensity in skeletal-muscle Mr images. Invest Radiol. 1990; 25(5):480–485. [PubMed: 2345077]
22. Weidman ER, Charles HC, Negrovilar R, Sullivan MJ, Macfall JR. Muscle-activity localization with P-31 spectroscopy and calculated T2-weighted h-1 images. Invest Radiol. 1991; 26(4):309–316. [PubMed: 2032818]
23. Adams GR, Duvoisin MR, Dudley GA. Magnetic-resonance-imaging and electromyography as indexes of muscle function. J Appl Physiol. 1992; 73(4):1578–1589. [PubMed: 1447107]
24. WOLFF S, BALABAN R. NMR imaging of labile proton-exchange. J Magn Reson. 1990; 86:164–169.
25. Guivel-Scharen V, Sinnwell T, Wolff S, Balaban R. Detection of proton chemical exchange between metabolites and water in biological tissues. J Magn Reson. 1998; 133:36–45. [PubMed: 9654466]
26. Ward K, Aletras A, Balaban R. A new class of contrast agents for MRI based on proton chemical exchange dependent saturation transfer (CEST). J Magn Reson. 2000; 143:79–87. [PubMed: 10698648]
27. Ward K, Balaban R. Determination of pH using water protons and chemical exchange dependent saturation transfer (CEST). Magn Reson Med. 2000; 44:799–802. [PubMed: 11064415]
28. Zhou J, Wilson D, Sun P, Klaus J, van Zijl P. Quantitative description of proton exchange processes between water and endogenous and exogenous agents for WEX, CEST, and APT experiments. Magn Reson Med. 2004; 51:945–952. [PubMed: 15122676]
29. Jones C, Schlosser M, van Zijl P, Pomper M, Golay X, Zhou J. Amide proton transfer imaging of human brain tumors at 3T. Magn Reson Med. 2006; 56:585–592. [PubMed: 16892186]
30. Zhou J, van Zijl P. Chemical exchange saturation transfer imaging and spectroscopy. Prog in Nuc Magn Reson Spectrosc. 2006; 48:109–136.
31. Cai K, Haris M, Singh A, Kogan F, Greenberg J, Hariharan H, Detre J, Reddy R. Magnetic resonance imaging of glutamate. Nat Med. 2012; 18(2):302–306. [PubMed: 22270722]
32. Sun P, Benner T, Kumar A, Sorensen A. Investigation of optimizing and translating pH-sensitive pulsed-chemical exchange saturation transfer (CEST) imaging to a 3T clinical scanner. Magn Reson Med. 2008; 60(4):834–841. [PubMed: 18816867]
33. Singh, A.; Haris, M.; Cai, K.; Hariharan, H.; Reddy, R. Chemical Exchange Transfer Imaging of Creatine. Proceedings of the 19th Annual Meating of ISMRM; Montreal, Canada. 2011. p. 2767
34. Haris M, Nanga RPR, Singh A, Cai K, Kogan F, Hariharan H, Reddy R. Exchange rates of creatine kinase metabolites: feasibility of imaging creatine by chemical exchange saturation transfer MRI. NMR Biomed. 2012; 25:1305–1309. [PubMed: 22431193]
35. Kim M, Gillen J, Landman B, Zhou J, van Zijl P. Water Saturation Shift Referencing (WASSR) for Chemical Exchange Saturation Transfer (CEST) Experiments. Magn Reson Med. 2009; 61:1441–1450. [PubMed: 19358232]
36. Singh A, Cai K, Haris M, Hariharan H, Reddy R. On B1 inhomogeneity correction of in vivo human brain glutamate chemical exchange saturation transfer contrast at 7T. Magn Reson Med. 2012 n/a-n/a.
37. Bottomley PA. Spatial localization in NMR-spectroscopy in vivo. Ann N Y Acad Sci. 1987; 508:333–348. [PubMed: 3326459]
38. Liu G, Gilad AA, Bulte JWM, van Zijl PCM, McMahon MT. High-throughput screening of chemical exchange saturation transfer MR contrast agents. Contrast Media Mol Imaging. 2010; 5(3):162–170. [PubMed: 20586030]
39. Iotti S, Lodi R, Frassineti C, Zaniol P, Barbiroli B. In-vivo assessment of mitochondrial functionality in human gastrocnemius-muscle by P-31 MRS - the role of pH in the evaluation of phosphocreatine and inorganic-phosphate recoveries from exercise. NMR Biomed. 1993; 6(4): 248–253. [PubMed: 8217526]

40. Robergs RA, Ghiasvand F, Parker D. Biochemistry of exercise-induced metabolic acidosis. Am J Physiol Regul Integr Comp Physiol. 2004; 287(3):502–516.

41. Rossiter HB, Ward SA, Howe FA, Kowalchuk JM, Griffiths JR, Whipp BJ. Dynamics of intramuscular P-31-MRS P-i peak splitting and the slow components of PCr and O-2 uptake during exercise. J Appl Physiol. 2002; 93(6):2059–2069. [PubMed: 12391122]

42. van Zijl PCM, Jones CK, Ren J, Malloy CR, Sherry AD. MR1 detection of glycogen in vivo by using chemical exchange saturation transfer imaging (glycoCEST). Proc Natl Acad Sci USA. 2007; 104:4359–4364. [PubMed: 17360529]

43. Arnold DL, Matthews PM, Radda GK. Metabolic recovery after exercise and the assessment of mitochondrial-function invivo in human skeletal-muscle by means of P-31 NMR. Magn Reson Med. 1984; 1(3):307–315. [PubMed: 6571561]

44. Sahlin K, Harris RC, Nylind B, Hultman E. Lactate content and pH in muscle samples obtained after dynamic exercise. Pflugers Arch. 1976; 367(2)

45. Zhou J, Lal B, Wilson D, Laterra J, van Zijl P. Amide proton transfer (APT) contrast for imaging of brain tumors. Magn Reson Med. 2003; 50:1120–1126. [PubMed: 14648559]

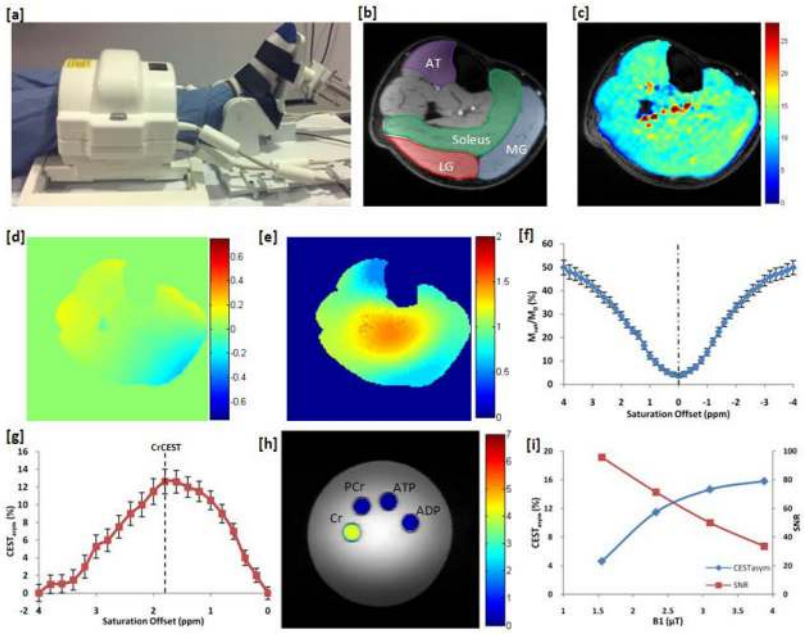

Figure 1.

CrCEST Mapping and B_1 Optimization. (**a**) In magnet exercise setup consisting of an MR compatible pneumatically driven pedal and a 28 channel knee coil for imaging of the lower leg. (**b**) Anatomical image with the major muscles [lateral gastrocnemius (LG), medial gastrocnemius (MG), soleus, and anterior tibialis (AT)] of the lower leg manually segmented. (**c**) $CrCEST_{asym}$ map at 7T, (**d**) local static magnetic field (B_0), and (**e**) radiofrequency field (B_1) maps of the lower leg. (**f,g**) The z-spectra and corresponding asymmetry plots for the soleus muscle at baseline. (**h**) Phantom containing of nmr tubes with solutions of 10 mM Cr, 15 mM PCr, 10 mM ATP, and 10 mM ADP immersed in a beaker containing PBS. CrCEST images were acquired around 1.8 ppm with a saturation pulse train with B_{1rms} = 123 Hz (2.9 μT) and a 500 ms duration. (**i**) Plot of the $CEST_{asym}$ as well as the signal-to-noise ratio (SNR) of the anatomical image following saturation as a function of saturation pulse B_{1rms} for a 500 ms pulse train used to empirically optimize CEST saturation parameters.

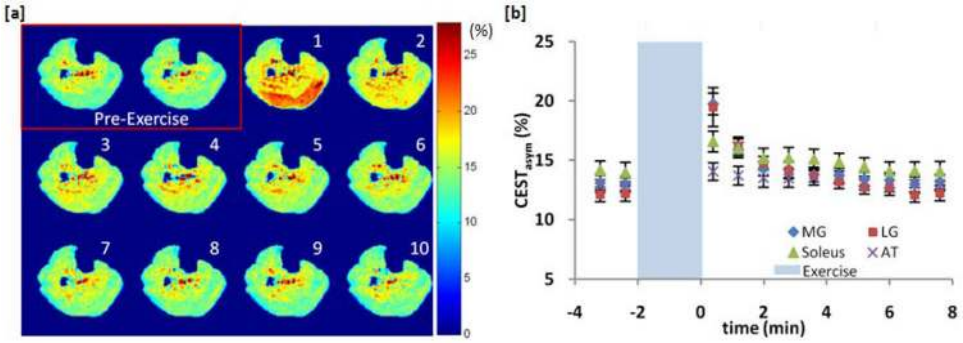

Figure 2.

Plantar flexion exercise data for subject 1. (**a**) $CrCEST_{asym}$ maps of a human calf muscle before and every 48 seconds after (in order by number) 2 minutes of plantar flexion exercise. Color bar represents $CrCEST_{asym}$ in percent. (**b**) Plot of the average $CrCEST_{asym}$ as function of time in 4 different muscles of the calf segmented from anatomical images. Error bars represent the standard deviation in the $CrCEST_{asym}$ in each region.

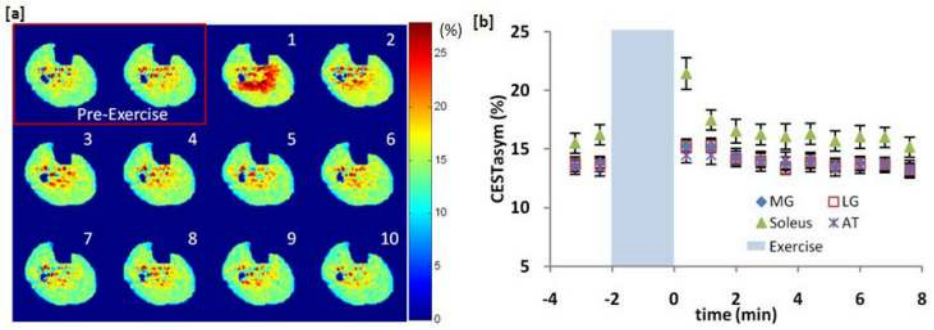

Figure 3.

Plantar flexion exercise data for subject 2 showing variability in muscle activation between subjects. (**a**) $CrCEST_{asym}$ maps before and every 48 seconds after (in order by number) 2 minutes of plantar flexion exercise. Color bar represents $CrCEST_{asym}$ in percent. (**b**) Plot of the average $CrCEST_{asym}$ as function of time in 4 different muscles of the calf segmented from anatomical images. Error bars represent the standard deviation in the $CrCEST_{asym}$ in each region.

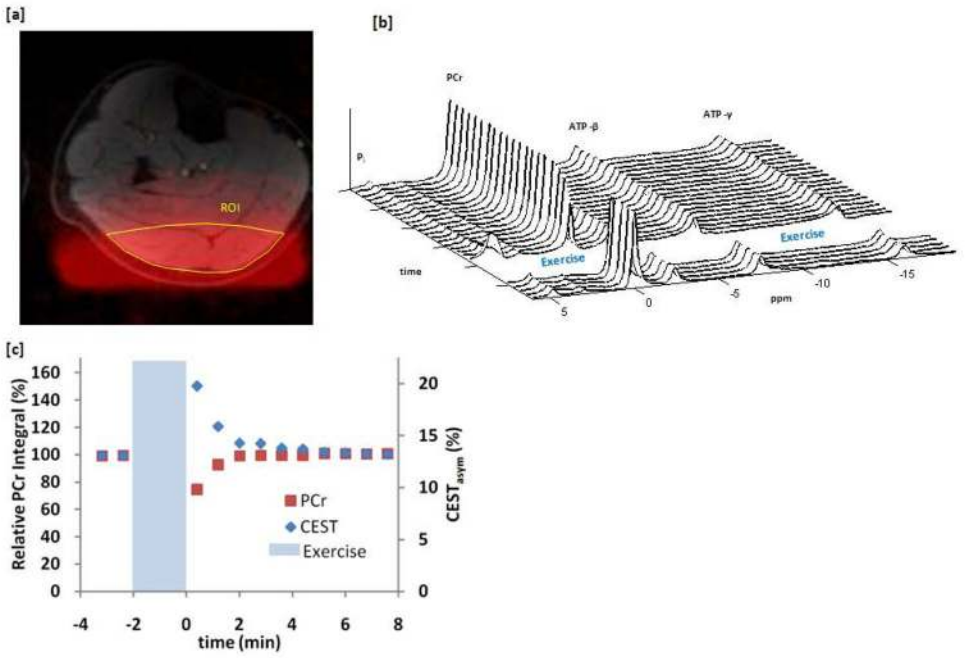

Figure 4.

^{31}P MRS data of the healthy human calf muscle before and after exercise. (**a**) Excitation profile of the ^{31}P surface coil (red) overlaid on an anatomical image of the lower leg with corresponding segmented CrCEST region of interest outlined in yellow. (**b**) Stacked plot of every alternate ^{31}P MRS spectra acquired 2 minutes before and 8 minutes after exercise. (**c**) Comparison between the $CrCEST_{asym}$ and ^{31}P MRS signal as a function of time at an equal temporal resolution of 48 seconds.

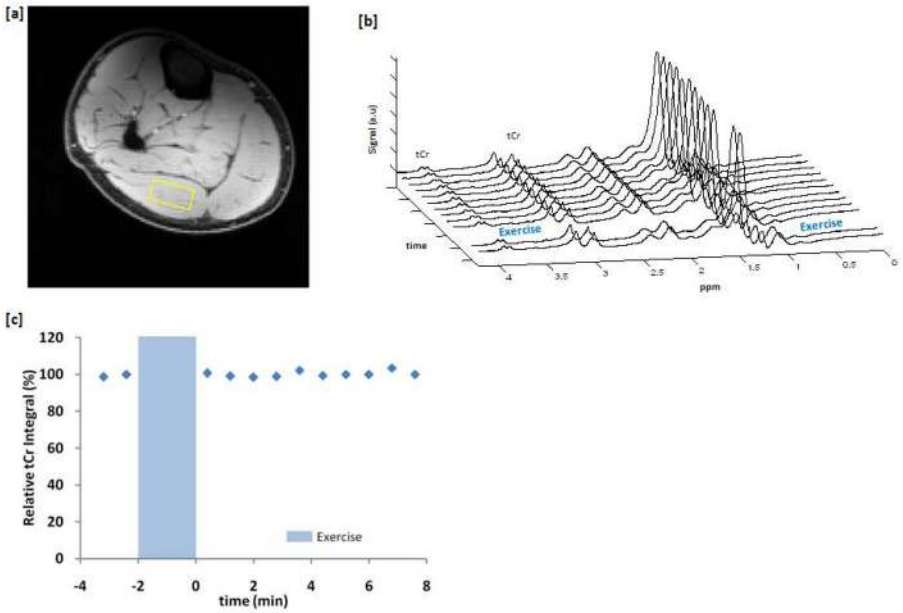

Figure 5.

^{1}H MRS data of the healthy human calf muscle before and after exercise. (**a**) Spectroscopy voxel location overlaid on the anatomical image. (**b**) ^{1}H MRS spectra 2 minutes before and 8 minutes after exercise with a temporal resolution of 48s. (**c**) No changes in the plot of tCr peak area as a function of time were observed.

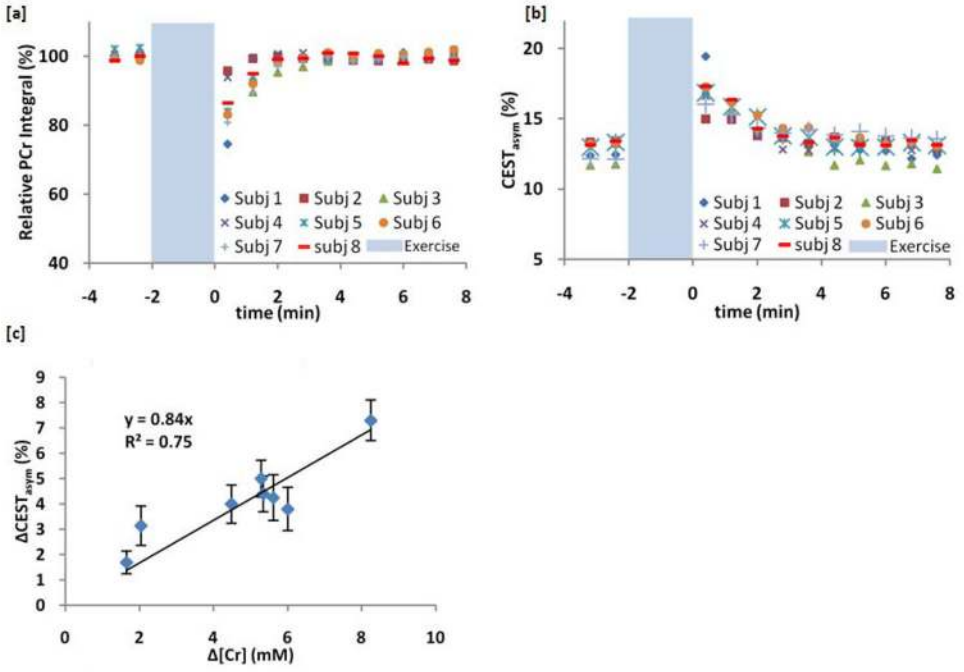

Figure 6.

$CrCEST_{asym}$ and ^{31}P MRS data across subjects. (**a**) ^{31}P MRS PCr peak integral as a function of time before and after exercise for all subjects with a 48 second temporal resolution. (**b**) The average $CrCEST_{asym}$ as a function of time for each subject in a region of interest selected to correlate to the depth of penetration of the ^{31}P MRS surface coil. (**c**) Comparison of changes in $CrCEST_{asym}$ Cr concentration following exercise. The % decrease in ^{31}P MRS signal from baseline at the first integrated measurement following exercise was used to determine the decrease in PCr based on a 33 mM PCr baseline concentration[8]. As the total Cr remains constant, the decrease in PCr concentration was equated to an equivalent increase in Cr concentration.